Supporting Information for

Tuning the selectivity of benzene hydroalkylation over the PdZn/HBeta catalysts: Identification on lattice contraction and electronic properties

Jie Feng,[†[a]] Qiaoyun Liu,[†[a]] Haojie Li,[[d]] Zhongxian Song,[[a]] Lin Dong,[[b]] Shufang Zhao,[[c]] Young Dok Kim,[*[c]] Zhongyi Liu,[*[a]] and Zhikun Peng[*[a]]

a. [a] *College of Chemistry, Research Center of Green Catalysis, Henan Institute of Advanced Technology, Zhengzhou University, Zhengzhou 450001, Henan, China.*

b. [b] *Beijing Institute of Nanoenergy and Nanosystems, Chinese Academy of Sciences, Beijing, 100083, China.*

c. [c] *Department of Chemistry, Sungkyunkwan University, Suwon, 16419, Republic of Korea.*

d. [d] *Interdisciplinary Research Center of Biology & Catalysis, School of Life Sciences, Northwestern Polytechnical University, Xi'an 710072, Shanxi, China.*

e. ** Corresponding author. E-mail: ydkim91@skku.edu*

f. ** Corresponding author. E-mail: liuzhongyi@zzu.edu.cn*

g. ** Corresponding author. E-mail: pengzhikun@zzu.edu.cn*

Materials

Palladium chloride (Pd 59-60%, $PdCl_2$, Aladdin), zinc chloride (98.5%, $ZnCl_2$, Nanjing Chemical Reagent Co., Ltd.), cupric chloride dihydrate (AR, $CuCl_2.2H_2O$, Macklin), nickel chloride hexahydrate (99%, $NiCl_2.6H_2O$, Macklin), cobalt chloride hexahydrate (99%, $CoCl_2.6H_2O$, SCR), ammonium chloride (99.5%, NH_4Cl, Macklin), benzene (99.5%, C_6H_6, SCR), cyclohexyl benzene (98%, $C_{12}H_{16}$, Adamas Reagent Co., Ltd), cyclohexene (AR, C_6H_{10}, Macklin), cyclohexane (99.7%, C_6H_{12}, Kermel), Na-Beta zeolite (SiO_2/Al_2O_3=30, Shandong HEFA Environmental Technology Co., Ltd.), silica fumed (SiO_2, Aladdin), alumina (99.9%, Al_2O_3, Aladdin), activated charcoal (C, Macklin).

Computational Details

The first-principles density functional theory (DFT) calculations was performed within the generalized gradient approximation (GGA) based on via Vienna abinitio simulation package (VASP) [1]. We constructed molecular models with periodicity in the x and y directions and the depth of the vacuum layer is greater than 15 Å in order to prevent self-interactions. The calculations were performed using the hybrid functional as proposed by Perdew-Burke-Ernzerhof (PBE) [1]. The interactions are represented using the projector augmented wave (PAW) [1, 2] potential, and the Kohn-Sham one-electron valence states were expanded on the basis of plane waves with a cutoff energy of 400 eV. The Hellmann-Feynman forces convergence criterion was set as less than 0.05 eV/Å. The K-point of 3×3×1 was used for the optimization of all molecular models.
Subsequently, we calculated the electrostatic potential, electron localization function (ELF) in the single point energy calculation. The electronic energy was considered self-consistent while the energy variation was smaller than 10^{-5} eV. The value of K-point, cutoff energy is the same as the process of structure optimization.

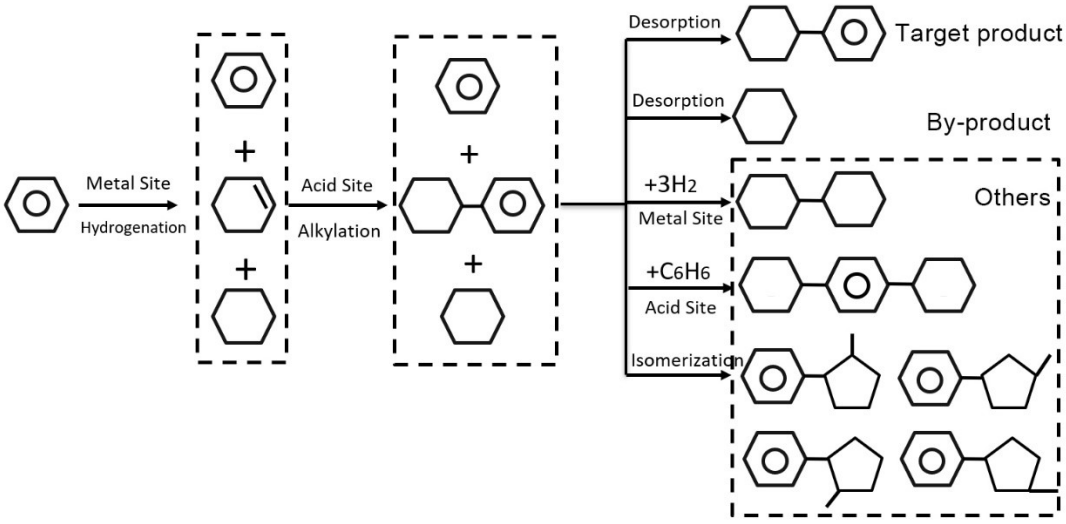

Scheme S1 Reaction network for the hydroalkylation of benzene.

As described in scheme S1, benzene can be hydrogenated into both cyclohexene (CHE) and cyclohexane (CHA) on the metal site. And CHE can react with benzene to form cyclohexylbenzene (CHB). The produced CHB can be further alkylated with CHE to form dicyclohexylbenzene (DCHB) or hydrogenated into bicyclohexyl. In addition, benzene and CHE can be isomerized on HBeta zeolite to form methylcyclopentylbenzene and its isomers as well.

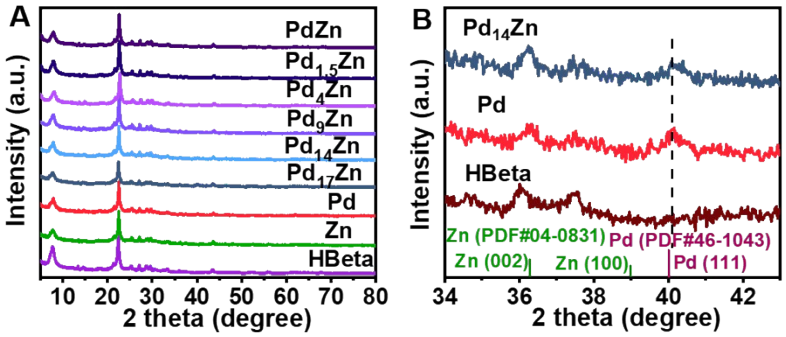

Fig. S1 (A) XRD patterns of HBeta, Zn/HBeta, Pd/HBeta and Pd_xZn/HBeta (x = 17, 14, 9, 4,1.5, 1). (B) Enlarged view selected from the XRD patterns of HBeta, Pd/HBeta and $Pd_{14}Zn$/HBeta.

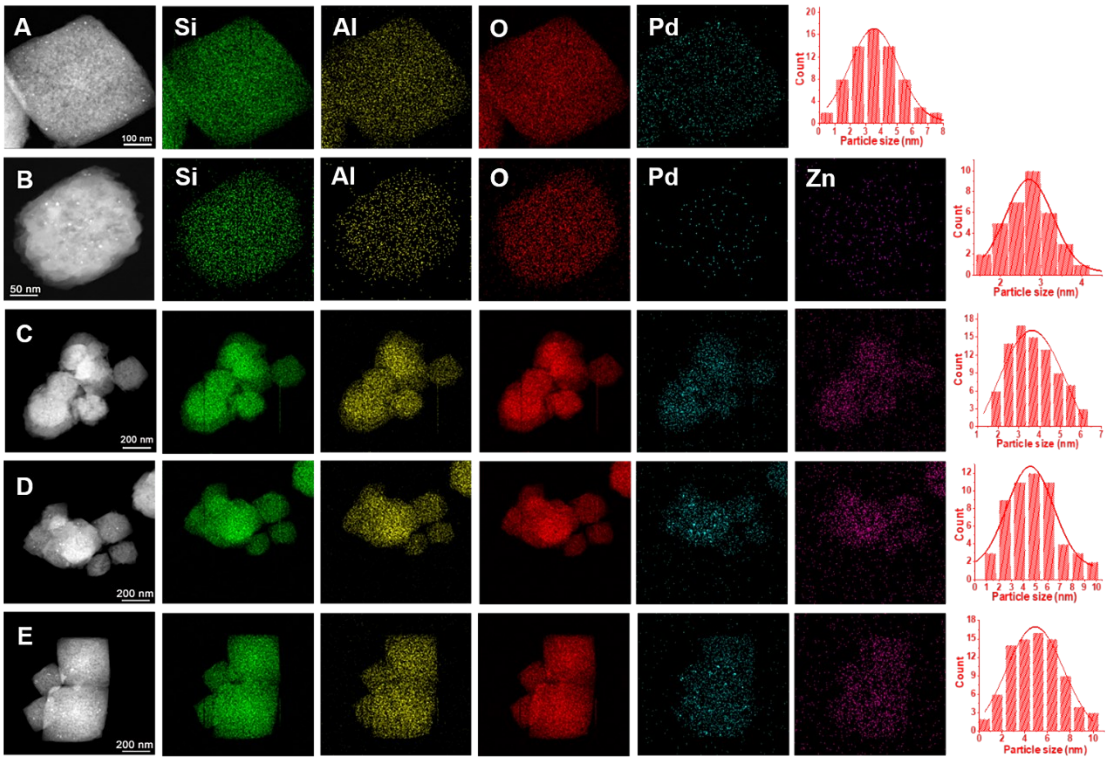

Fig. S2 TEM image and EDX mapping of (A) Pd/HBeta, (B) $Pd_{17}Zn$/HBeta, (C) Pd_9Zn/HBeta, (D) Pd_4Zn/HBeta, (E) PdZn/HBeta.

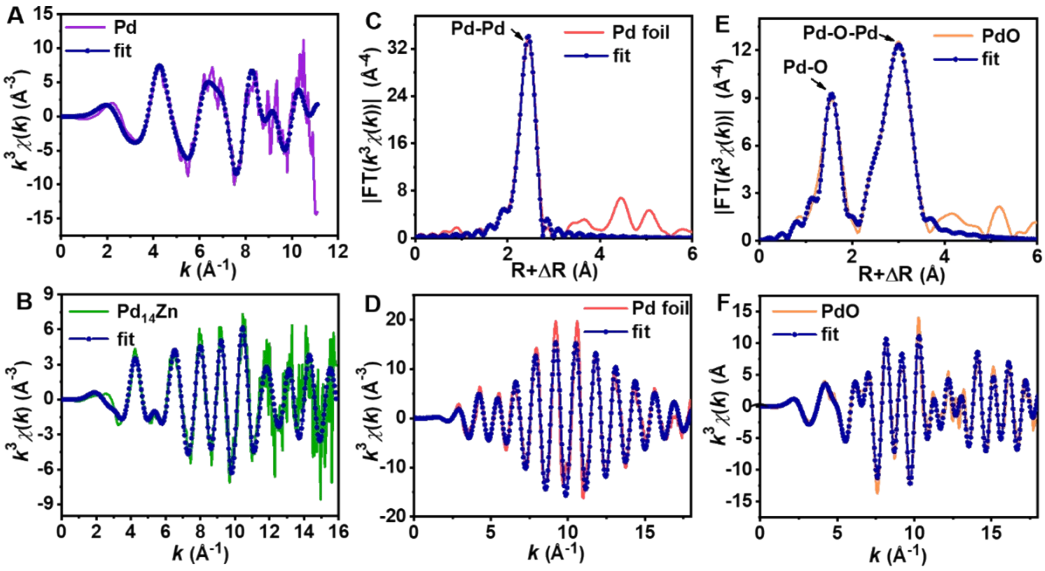

Fig. S3 FT-EXAFS fitting curves in K spaces for (A) Pd/HBeta and (B) $Pd_{14}Zn$/Hbeta. The reference samples in R spaces for (C) Pd foil and (E) PdO. The reference samples in K spaces for (D) Pd foil and (F) PdO.

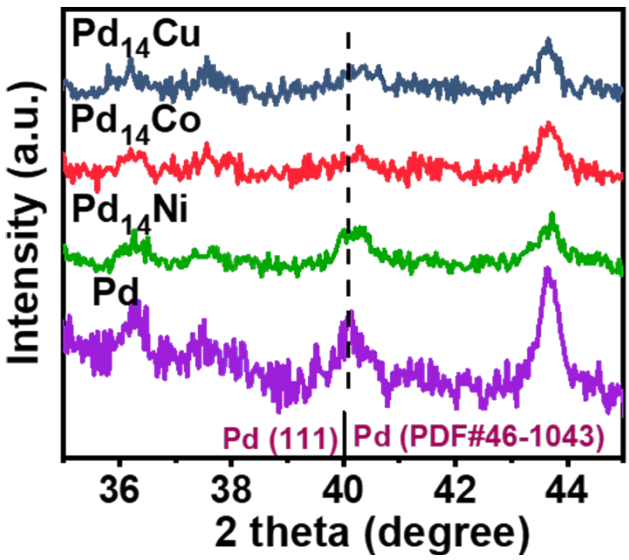

Fig. S4 XRD patterns of HBeta and $Pd_{14}M$/HBeta (M = Ni，Co，Cu).

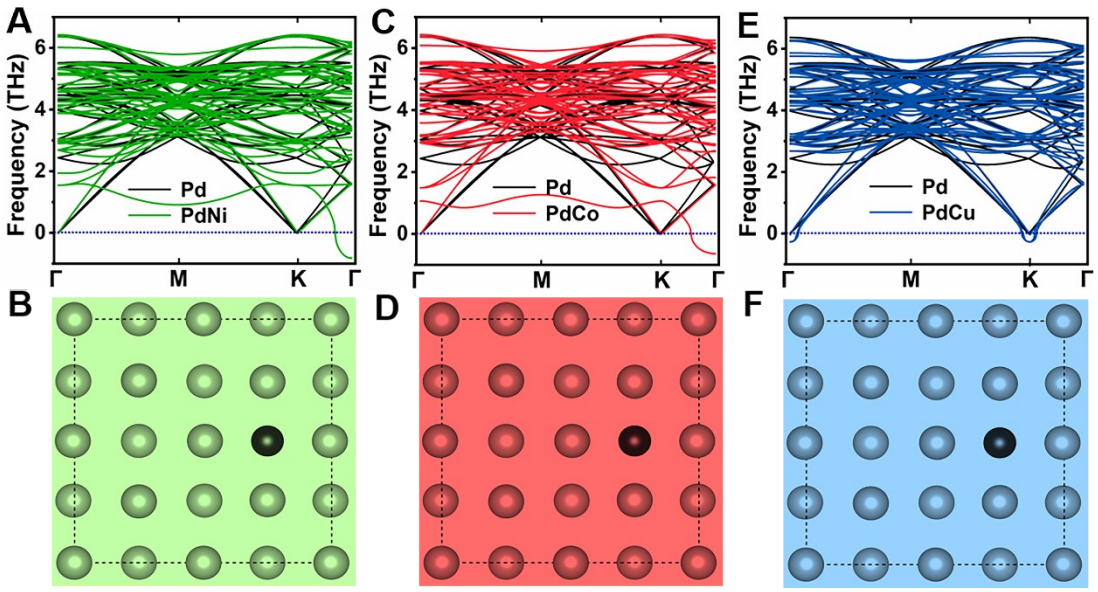

Fig. S5 (A) The phonon dispersions and (B) computational model of PdNi. (C) The phonon dispersions and (D) computational model of PdCo. (E) The phonon dispersions and (F) computational model of PdCu.

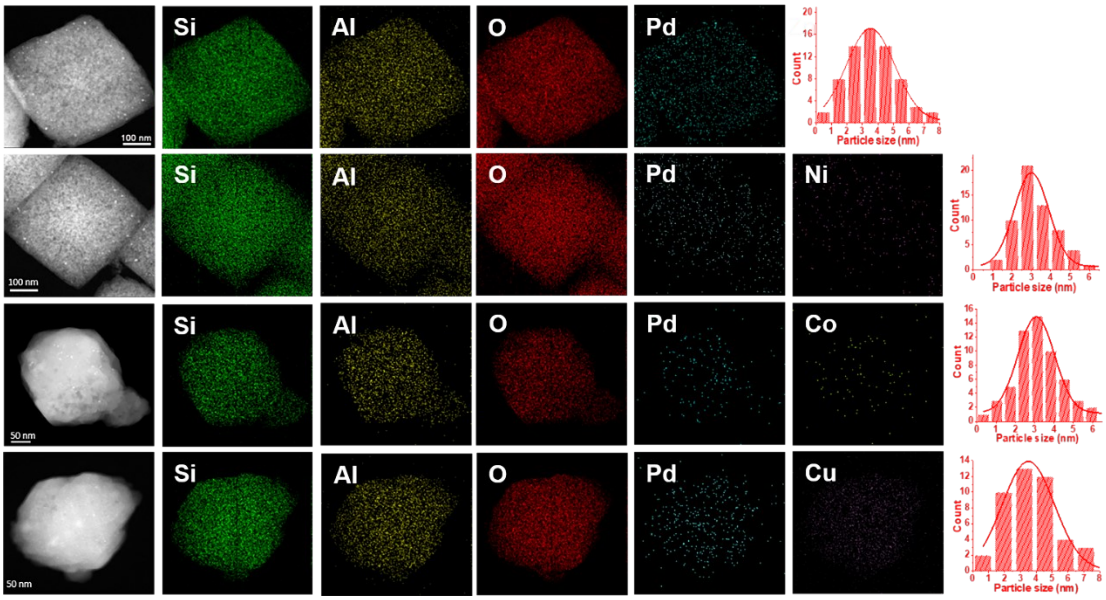

Fig. S6 TEM image and EDX mapping of the Pd/HBeta and Pd_{14}M/HBeta (M = Ni, Co or Cu).

Inductively coupled plasma optical emission spectrometer (ICP-OES) analysis reveals Pd_{14}M/HBeta has very stable metallic composition. The Pd content is in a narrow range between 0.69 to 0.75 wt%, and additive M is 0.03 wt% (**Table 1**). The XRD diffraction peaks of Pd_{14}M/HBeta also show the diffraction pattern of PdM NPs slightly shifted to higher 2 theta angles than that of pure Pd, revealing the successful doping of M into the Pd lattice structure (**Fig. S4**). The phonon vibration frequency of PdM (Ni, Co or Cu) increases obviously compared with that of Pd (**Fig. S5**), suggesting that the doping of M causes the lattice contraction of Pd. In addition, no virtual frequency in the phonon spectrum of PdZn were found, indicating that its surface are relatively stable [3]. As **Fig. S6** illustrated, Pd and PdM (Ni, Co or Cu) NPs were uniformly dispersed, and the mean diameter of the PdM NPs was about 3 nm, slightly smaller than that of Pd NPs of Pd/HBeta. Meanwhile, the dispersion of Pd on the catalyst increases slightly with the introduction of transition metal, indicating the exist of higher exposed and better dispersed PdM NPs for Pd_{14}M/HBeta catalysts (**Table 1**), which is consistence with the TEM results.

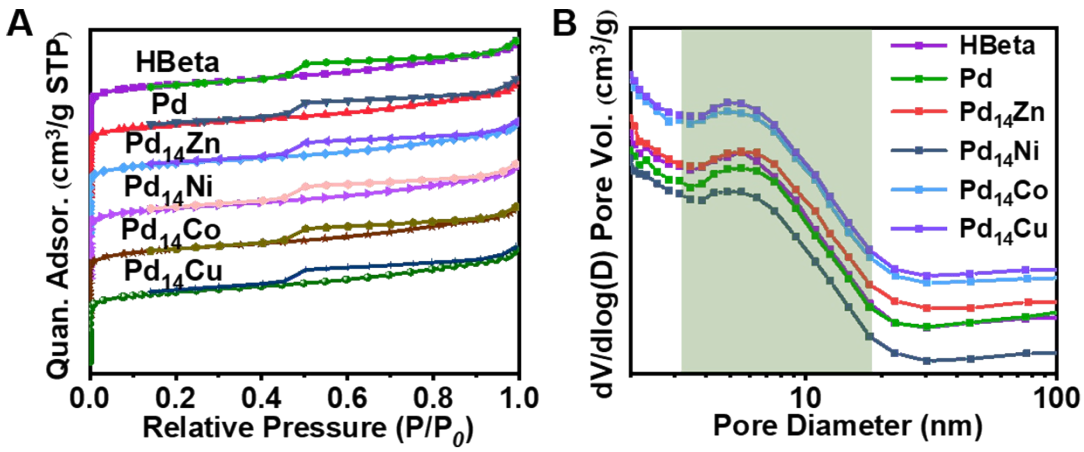

Fig. S7 (A) N_2 adsorption-desorption isotherms and (B) BJH pore size distribution of HBeta, Pd/HBeta and $Pd_{14}M$/HBeta (M = Zn, Ni, Co or Cu).

The N_2 adsorption and desorption isotherms of $Pd_{14}M$/HBeta catalysts as well as HBeta and Pd/HBeta were shown in **Fig. S7A**. It can be seen that all the samples exhibit typical- IV isotherm curves related to the presence of mesoporosity, according to the IUPAC classification [4]. BJH pore size distribution also demonstrates the existence of mesopores existed in all the samples (**Fig. S7B**). The adsorption amount of N_2 is large in the lower partial pressure ($P/P_0 \leqq 0.2$), indicating the presence of micropores [5]. The similar texture properties of $Pd_{14}M$/HBeta catalysts confirmed that the introduction of M has little effect on the pore structure parameters of HBeta.

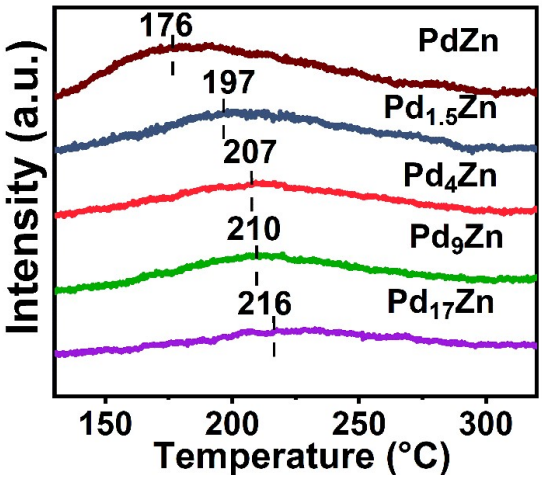

Fig. S8 H_2-TPD desorption spectra of Pd_xZn/HBeta (x = 17, 9, 4, 1.5, 1).

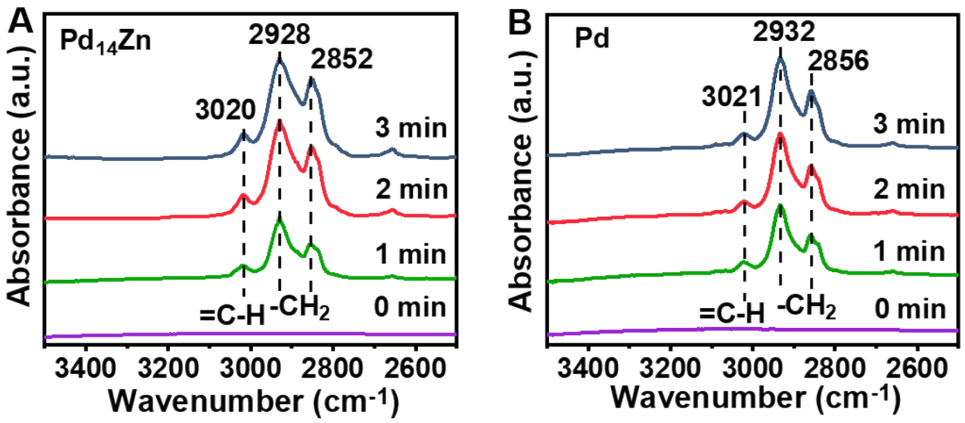

Fig. S9 In-situ DRIFTS spectra for CHE adsorption on (A) $Pd_{14}Zn$/HBeta and (B) Pd/HBeta at 25 ℃.

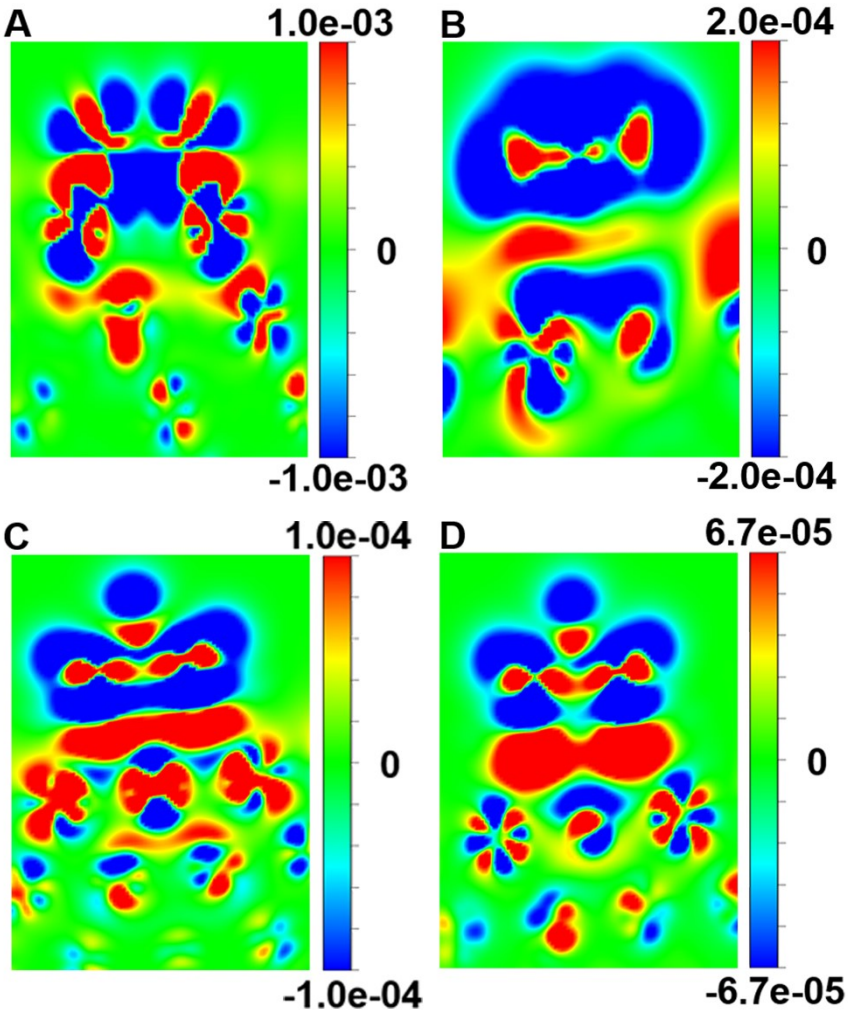

Fig. S10 A two-dimensional slice differential charge density diagram of benzene on (A) a pristine Pd and (B) a Zn-doped Pd, CHE on (C) a pristine Pd and (D) a Zn-doped Pd.

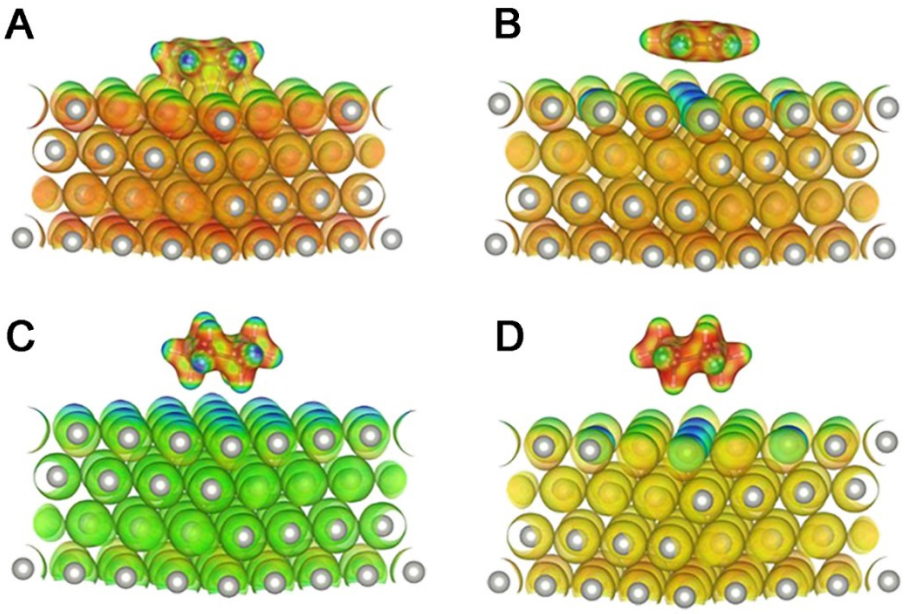

Fig. S11 Electrostatic potential distribution of benzene on (A) a pristine Pd and (B) a Zn-doped Pd, CHE on (C) a pristine Pd and (D) a Zn-doped Pd.

Table S1 Structure parameters of Pd and PdM (Zn, Ni, Co or Cu).

sample	a/Å	b/Å	c/Å
Pd	7.88	7.88	3.94
PdZn	7.87	7.87	3.92
PdNi	7.84	7.84	3.91
PdCo	7.84	7.84	3.91
PdCu	7.85	7.85	3.92

Table S2 EXAFS fitting parameters at the Pd K-edge for references, $Pd_{14}Zn$/HBeta and Pd/HBeta (S_0^2 = 0.844).

Sample	Shell	*CN*[a]	*R*(Å)[b]	σ^2(Å^2)[c]	ΔE_0(eV)[d]	*R* factor
Pd foil	Pd-Pd	12*	2.74	0.0056	-6.2	0.0046
PdO	Pd-O	4.1	2.01	0.0017	-2.6	0.0013
	Pd-O-Pd	5.1	3.05	0.0049		
	Pd-O-Pd	6.4	3.43	0.0036		
Pd	Pd-O	6.8	1.96	0.0046	-5.6	0.0092
	Pd-Pd	1.1	2.65	0.0061		
	Pd-O-Pd	4.0	3.41	0.0061		
$Pd_{14}Zn$	Pd-O	2.8	2.02	0.0045	-4.0	0.0061
	Pd-Zn	0.6	2.51	0.0085		
	Pd-Pd	2.9	2.75	0.0085		
	Pd-O-Pd	1.4	3.39	0.0085		

[a] *CN*, coordination number. [b] *R*, distance between absorber and backscatter atoms. [c] σ^2, Debye-Waller factor to account for both thermal and structural disorders. [d] ΔE_0, inner potential correction. *R* factor indicates the goodness of the fit. Error bounds (accuracies) that characterize the structural parameters obtained by EXAFS spectroscopy were estimated as N ± 20%, R ± 1%, σ^2 ± 20%, ΔE_0 ± 20%. S_0^2 was fixed to 0.844, according to the experimental EXAFS fit of Pd foil by fixing CN as the known crystallographic value. Fitting range: 3.0 ≤ *k* (/Å) ≤ 16.2 and 1.0 ≤ *R* (Å) ≤ 3.0 (Pd foil), 3.0 ≤ *k* (/Å) ≤ 13.3 and 1.0 ≤ *R* (Å) ≤ 3.8 (PdO), 3.0 ≤ *k* (/Å) ≤ 12.1 and 1.0 ≤ *R* (Å) ≤ 3.0 (Pd). A reasonable range of EXAFS fitting parameters: 0.700 < S_0^2 < 1.000, *CN* > 0, σ^2 > 0 Å^2, $|\Delta E_0|$ < 10 eV, *R* factor < 0.02.

Table S3 Pore structure parameters of HBeta, Pd/HBeta and $Pd_{14}M$/HBeta (Zn, Ni, Co or Cu).

Sample	S_{BET} (m^2/g)	V_{tot} (cm^3/g)	V_{micro} (cm^3/g)	D_{avg}/nm
HBeta	547.64	0.39	0.17	4.83
Pd	516.21	0.38	0.17	4.99
$Pd_{14}Zn$	545.66	0.36	0.17	4.80
$Pd_{14}Ni$	573.23	0.38	0.16	4.80
$Pd_{14}Co$	573.80	0.37	0.16	4.77
$Pd_{14}Cu$	541.76	0.37	0.16	4.82

Table S4 Benzene HDA reaction over various catalysts.

Entry	Catalyst[a]	Reaction Rate	Conversion	Selectivity (mol. %)			Yields (%)
		(mmol/g/h)	(mol. %)	CHA	CHB	Others	CHB
1	HBeta	0	0	0	0	0	0
2	Zn/HBeta	0	0	0	0	0	0
3	Pd/HBeta	273.3	97.3	84.7	6.9	8.4	6.7
4	$Pd_{14}Zn$/HBeta	247.1	88.0	66.2	22.0	11.9	19.3
5	$Pd_{14}Zn$/dealumination HBeta	31.9	11.4	69.7	0	30.3	0
6	Pd/C	0	0	0	0	0	0
7	Pd/SiO_2	0	0	0	0	0	0

[a] Reaction Condition: 0.5 g of catalyst, 280.9 mmol of benzene, 4.0 MPa H_2, T = 200 °C, t = 120 min, and a stirring rate of 500 rpm.

Reference

1 W. Li, F. Wang, X. Liu, Y. Dang, J. Li, T. Ma and C. Wang, *Appl. Catal. B-Environ.*, 2022, **313**, 121470.
2 M. Engel, M. Marsman, C. Franchini and G. Kresse, *Phys. Rev. B*, 2020, **101**, 184302.
3 X. Wang, M. Wu, T. Yang and R. Khenata, *RSC Adv.*, 2020, **10**, 17829-17835.
4 M. Thommes, K. Kaneko, A. V. Neimark, J. P. Olivier, F. Rodriguez-Reinoso, J. Rouquerol and K. S. W. Sing, *Pure Appl. Chem.*, 2015, **87**, 1051-1069.
5 J. Jagiello, A. Chojnacka, S. E. M. Pourhosseini, Z. Wang and F. Beguin, *Carbon*, 2021, **178**, 113-124.